FGF Regulates TGF-# Signaling and Endothelial-to-Mesenchymal Transition via Control of let-7 miRNA Expression

Citation: Chen, Pei-Yu, Lingfeng Qin, Carmen Barnes, Klaus Charisse, Tai Yi, Xinbo Zhang, Rahmat Ali, et al. "FGF Regulates TGF-ß Signaling and Endothelial-to-Mesenchymal Transition via Control of Let-7 miRNA Expression." Cell Reports 2, no. 6 (December 2012): 1684–1696.

As Published: http://dx.doi.org/10.1016/j.celrep.2012.10.021

Publisher: Elsevier

Persistent URL: http://hdl.handle.net/1721.1/91896

Version: Final published version: final published article, as it appeared in a journal, conference proceedings, or other formally published context

Cell Reports
Article

FGF Regulates TGF-β Signaling and Endothelial-to-Mesenchymal Transition via Control of *let-7* miRNA Expression

Pei-Yu Chen,[1,10] Lingfeng Qin,[2,10] Carmen Barnes,[4,11] Klaus Charisse,[4] Tai Yi,[2] Xinbo Zhang,[1] Rahmat Ali,[2] Pedro P. Medina,[5] Jun Yu,[1] Frank J. Slack,[5] Daniel G. Anderson,[6,7,8] Victor Kotelianski,[6] Fen Wang,[9] George Tellides,[2] and Michael Simons[1,3,*]

[1]Yale Cardiovascular Research Center, Section of Cardiovascular Medicine, Department of Internal Medicine
[2]Department of Surgery
[3]Department of Cell Biology
Yale University School of Medicine, New Haven, CT 06520, USA
[4]Alnylam Pharmaceuticals Inc., 300 3rd Street, Cambridge, MA 02142, USA
[5]Department of Molecular, Cellular and Developmental Biology, Yale University, New Haven, CT 06520, USA
[6]Department of Chemical Engineering
[7]David H. Koch Institute for Integrative Cancer Research
[8]Harvard-MIT Division of Health Science and Technology
Massachusetts Institute of Technology, Cambridge, MA 02139, USA
[9]Texas A&M Health Science Center, Houston, TX 77030, USA
[10]These authors contributed equally to this work
[11]Present address: Celgene Avilomics Research, Bedford, MA 01730, USA
*Correspondence: michael.simons@yale.edu
http://dx.doi.org/10.1016/j.celrep.2012.10.021

SUMMARY

Maintenance of normal endothelial function is critical to various aspects of blood vessel function, but its regulation is poorly understood. In this study, we show that disruption of baseline fibroblast growth factor (FGF) signaling to the endothelium leads to a dramatic reduction in *let-7* miRNA levels that, in turn, increases expression of transforming growth factor (TGF)-β ligands and receptors and activation of TGF-β signaling, leading to endothelial-to-mesenchymal transition (Endo-MT). We also find that Endo-MT is an important driver of neointima formation in a murine transplant arteriopathy model and in rejection of human transplant lesions. The decline in endothelial FGF signaling input is due to the appearance of an FGF resistance state that is characterized by inflammation-dependent reduction in expression and activation of key components of the FGF signaling cascade. These results establish FGF signaling as a critical factor in maintenance of endothelial homeostasis and point to an unexpected role of Endo-MT in vascular pathology.

INTRODUCTION

Maintenance of the normal vasculature is an active process. Fibroblast growth factors (FGFs) have recently emerged as key regulators of the normal vascular state (Hatanaka et al., 2011; Murakami et al., 2008). Circulating and tissue-resident FGF signal via cognate tyrosine kinase receptors that require the intracellular adaptor FRS2 for the initiation of mitogen-activated protein kinase (MAPK) signaling (Eswarakumar et al., 2005). Experimental evidence using various in vitro models points to FGF's role in inhibition of TGF-β signaling. Thus, FGF2 downregulates TGF-βR1 expression, attenuates endothelial cell (EC) responses to TGF-β (Fafeur et al., 1990), and antagonizes TGF-β1-mediated smooth muscle α-actin (αSMA) expression (Papetti et al., 2003). In addition, FGF can revert TGF-β1-induced epithelial-to-mesenchymal transition (EMT) in epithelial cells via the MAPK pathway (Ramos et al., 2010). These observations suggest that loss of endothelial FGF signaling may lead to upregulation of the TGF-β pathway and promotion of adverse changes in the vasculature. However, the molecular mechanisms linking FGF and TGF-β signaling cascades and the biological role of FGF-dependent regulation of TGF-β signaling have not been identified.

One likely consequence of dysregulated TGF-β signaling in the vasculature is the development of neointima. Neointima formation underlies a number of common diseases including transplant vasculopathy, postangioplasty, and vascular graft restenosis, hypertension, and atherosclerosis among others. Despite decades of investigations, the origins of neointimal cells still remains controversial with studies variously pointing to the role of medial smooth muscle cell (SMC) proliferation (Costa and Simon, 2005), vessel wall inflammation (Ohtani et al., 2004), and adventitial angiogenesis (Khurana et al., 2004).

One potential contributor to neointima formation is the process of endothelial-to-mesenchymal transition (Endo-MT). Somewhat similar to EMT, Endo-MT is thought to result in endothelial cells *trans*-differentiating into mesenchymal cell types, including SMC-like and fibroblast-like cells. While Endo-MT

has been implicated in several pathological processes including cardiac fibrosis (Zeisberg et al., 2007b) and pulmonary hypertension (Kitao et al., 2009), its very existence is still controversial. Similarly to EMT, Endo-MT is thought to be driven by TGF-β in a SMAD-dependent and independent manner (Kitao et al., 2009; Medici et al., 2011). However, factors leading to Endo-MT under pathologic conditions or suppressing its occurrence in the normal vasculature have not been identified.

In this study, we observed that a shutdown of endothelial FGF signaling in normal ECs results in increased expression of TGF-β ligands and receptors and activation of TGF-β signaling. In vitro this resulted in a change in EC morphology and expression of SMC markers. In vivo, using fate-mapped mice, we observed neointima formation and extensive perivascular fibrosis. The process was driven by a decline in endothelial expression of *let-7* miRNAs that normally maintain low levels of TGF-βR1 expression. The effects of FGF signaling shutdown on Endo-MT induction could be mimicked by inhibition of *let-7b* or *let-7c* expression in vitro and in vivo. Endo-MT was a critical driver of neointima formation in a transplant arteriopathy model in mice, was present in rejecting human transplants, and could be reversed by treatment with *let-7*b mimics. These results demonstrate that basal FGF signaling is required to maintain high *let-7* expression in the endothelium that in turn prevents activation of TGF-β signaling and suppresses Endo-MT.

RESULTS

Basal FGF Signaling Suppresses TGF-β-Mediated Endo-MT

To test the role of FGF signaling in ECs, we used RNA interference in human umbilical artery endothelial cells (HUAECs) to inhibit expression of FRS2, the key adaptor molecule involved in FGF receptors signaling. Immunofluorescence staining showed that while control HUAECs display a typical rounded/cobblestone morphology, FRS2 knockdown resulted in a distinct change in cell shape accompanied by expression of smooth muscle calponin (SM-calponin), a protein not normally expressed in the endothelium (Figure 1A). Western blotting confirmed the appearance of this and other SMC markers in FRS2 knockdown cells (Figure 1B). Fluorescence-activated cell sorting analysis showed that both control and FRS2 knockdown ECs expressed CD31 and were able to take up Di-acLDL, ruling out SMC contamination (Figure 1C).

These findings suggest that following FRS2 knockdown ECs are undergoing Endo-MT as defined by an acquisition of mesenchymal markers. Since TGF-β signaling has been implicated in this process, we next examined *TGF-β*-related gene expression. Quantitative real-time PCR analysis demonstrated a marked increase in *TGF-β1* and *TGF-β2*, all three *TGF-β* receptors, as well as several collagen isoforms and other matrix proteins that are stimulated by TGF-β signaling (Figures 1D and 1E). Western blotting confirmed increased TGF-βR1 expression and activation of TGF-β signaling (Figure 1F). To verify that disruption of FGF signaling induces TGF-β signaling and Endo-MT, HUAECs were transduced with mutant forms of FRS2 that inhibit FGF signaling or with a dominant negative FGFR1 (FGFR1-DN) (Figure S1A). A complete suppression of FGF signaling achieved with expression of FGFR1-DN or *Frs2α*-6F constructs resulted in increased TGF-β signaling (Figure S1B) and an increase in smooth muscle and other mesenchymal marker expression (Figure S1C).

To demonstrate that activation of TGF-β signaling following FRS2 knockdown is indeed necessary and sufficient for Endo-MT, several different experimental approaches were used. Treatment of FRS2 knockdown ECs with the TGF-βR1 inhibitor SB431542 significantly decreased SM-calponin, fibronectin, and vimentin expression (Figure 1G). Similar results were seen after transduction of a dominant negative TGF-βR1 construct (TGF-βR1 K230R) (Figure 1H), while silencing SMAD2 expression with a specific small hairpin RNA resulted in a significant decrease in SM-calponin, but not in fibronectin and vimentin expression (Figure 1I). Finally, activation of TGF-β signaling in the absence of FGF signaling suppression was achieved by introduction of the wild-type TGF-βR1 together with TGF-β or by expression of a constitutively active TGF-βR1 (TGF-βR1-T202D) into HUAECs with a kinase dead mutant TGF-βR1-K230R used as a control (Figures S2A and S2B). Thus achieved, activation of TGF-β signaling resulted in increased expression of smooth muscle (Figure S2C) and other mesenchymal markers (Figure S2D).

FGF Controls TGF-βR1 Signaling via Regulation of *let-7* miRNA Expression

We next examined the mechanism responsible for increased expression of TGF-βR1 following FGF signaling shutdown. Analyses of mRNA half-life showed a marked increase following a knockdown of FRS2 expression (Figure 2A). This suggests the presence of miRNA regulating *TGFβR1* message stability. In silico analysis identified binding sites for the *let-7* family of miRNAs with an exact match to the seed sequence of *let-7* in *TGFβR1* 3′ UTR 75–82 and 3889–3895 (Figure 2B). At the same time, miRNA array analysis demonstrated a >20-fold reduction in expression of all *let-7* family members (with let-7b and 7c reduced 108- and 120-fold, respectively) following FRS2 knockdown in ECs (Figure 2C).

To demonstrate that increased TGF-β signaling following FGF suppression is directly due to changes in *let-7* levels, we inhibited *let-7* expression using two alternative approaches. Transduction of human umbilical vein endothelial cells (HUVECs) with LIN28, a known regulator of *let-7* biogenesis during embryonic development (Viswanathan and Daley, 2010), resulted in increased expression of genes in the *TGFβ* pathway and smooth muscle and mesenchymal markers (Figures 2D, left panel, and S3). Similarly, HUVEC transduction with a *let-7* "microsponge" construct that effectively suppresses expression of all *let-7* miRNAs also led to a marked increase in *TGFβR1*, SM-calponin, and *HMGA2* (a known *let-7* target) expression (Figure 2D, right panel).

We then examined if restoration of *let-7* expression in ECs with suppressed FGF signaling would, in turn, inhibit activation of TGF-β signaling and Endo-MT induction. To this end, HUAECs were transduced with *let-7*b or *let-7*c pre-miRs. Increased TGF-βR1 expression and SMAD2 phosphorylation induced by FRS2 knockdown were completely reversed by transduction with either *let-7*b or *let-7*c as was the expression of all Endo-MT markers (Figures 2E and 2F).

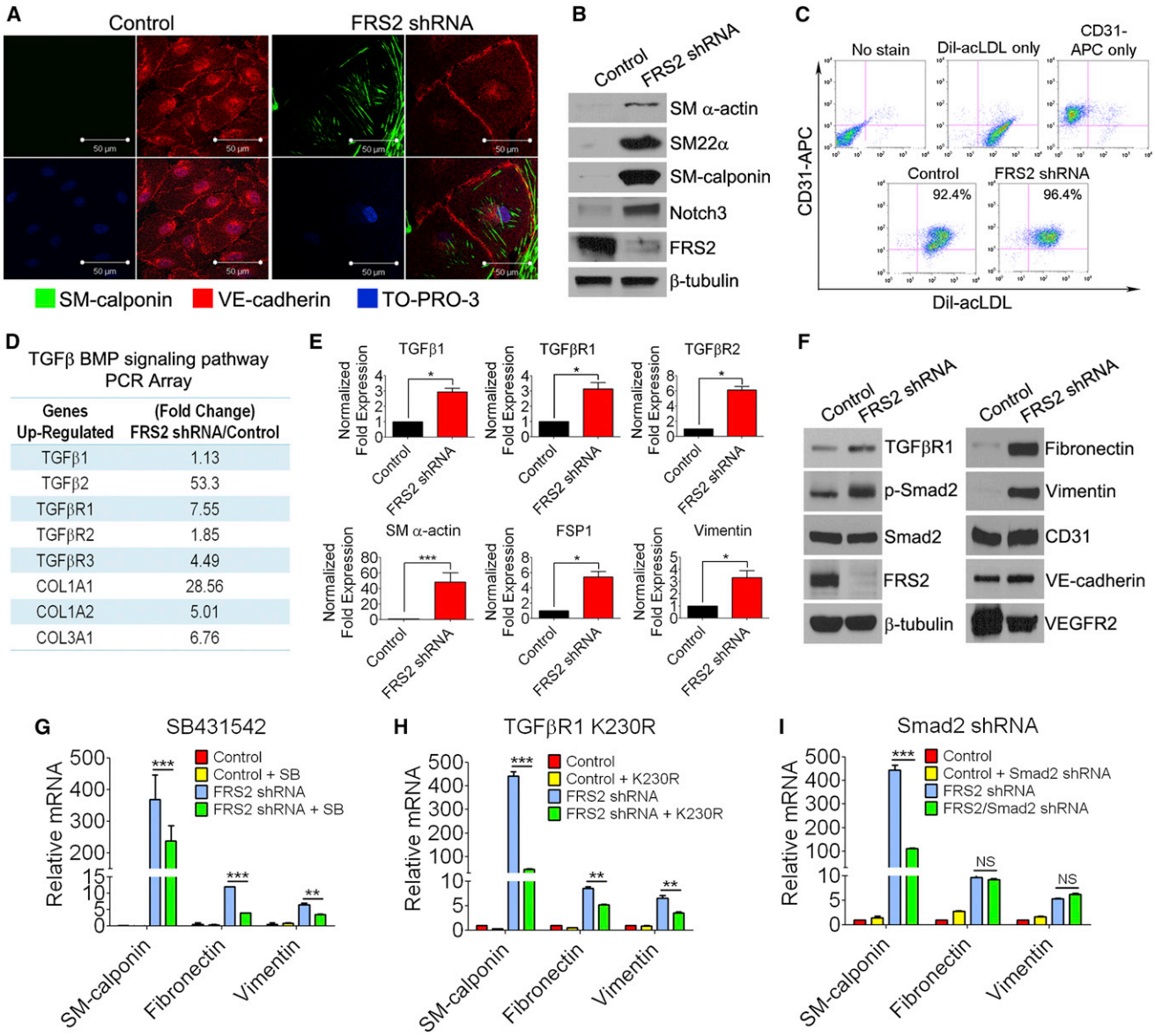

Figure 1. FRS2 Regulates Mesenchymal Marker Gene Expression via the TGF-βR1 Pathway

(A) Immunofluorescence staining of VE-cadherin (red) and SM-calponin (green) in control and FRS2 knockdown HUAECs. Nuclei were counterstained with TO-PRO-3 (blue). Scale bar: 50 μm.

(B) Immunoblots of SMC markers in control and FRS2 knockdown HUAECs.

(C) Control or FRS2 knockdown HUAECs were analyzed by flow cytometry for CD31 and Dil-acLDL.

(D) Quantitative real-time PCR array mRNA expression profile of TGF-β family genes from control or FRS2 knockdown cells.

(E) Quantitative real-time PCR analysis of TGF-βRs and downstream target gene expression in control and FRS2 knockdown HUAECs. Data are presented as mean ± SD, and two group comparisons were done with a two-tailed Student's t test (*$p < 0.05$; ***$p < 0.001$ compared to control). β-actin was used to normalize the variability in template loading.

(F) Immunoblots of TGF-βR1, Smad2, mesenchymal, and endothelial cell markers in control and FRS2 knockdown HUAECs.

(G–I) Quantitative real-time PCR analysis of SM-calponin and mesenchymal markers fibronectin and vimentin expression. Data are presented as mean ± SD, and two group comparisons were done with a two-tailed Student's t test (**$p < 0.01$; ***$p < 0.001$). β-actin was used to normalize the variability in template loading. Data shown are representative of four independent experiments (except D). NS, not significant compared to control. See also Figures S1 and S2.

The link between FGF signaling and *let-7* expression was then studied in vivo. Replacement of specific tyrosines in FRS2 (FRS2α-2F) (Figure S1A) that are phosphorylated by FGF biding to FGFR1 and activate ERK signaling results in a marked reduction in FGF signaling and embryonic lethality (Gotoh et al., 2004). Examination of *Frs2α-2F* embryos at E10.5 demonstrated a gene dose-dependent reduction in *let-7* levels (Figure S4A).

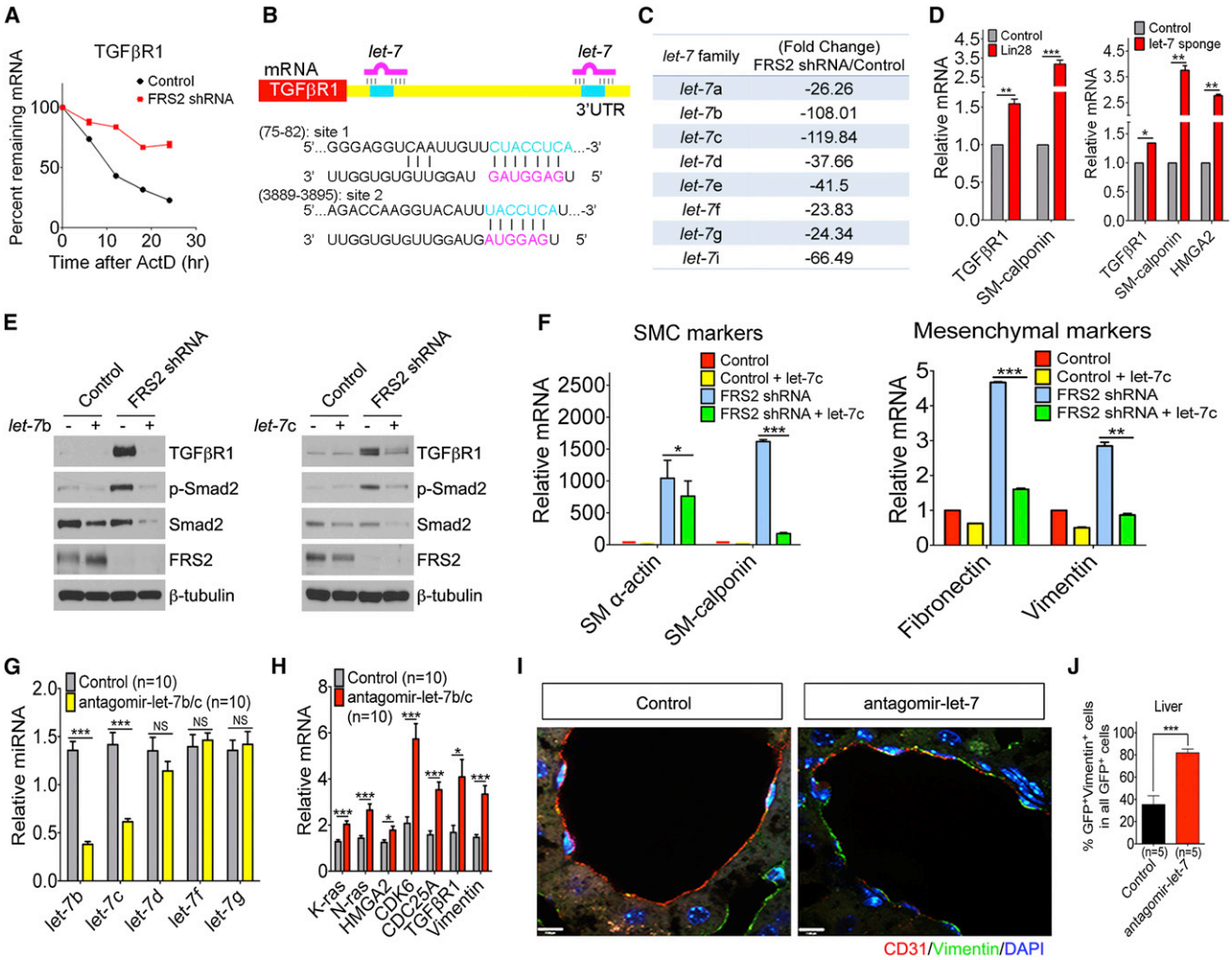

Figure 2. FRS2 Knockdown Downregulates let-7 Family

(A) Control or FRS2 knockdown HUAECs were treated with DMSO or 10 μg/ml actinomycin D (ActD) for the indicated times. Quantitative real-time PCR was then used to determine TGF-βR1 expression. 18S rRNA was used to normalize the variability in template loading.

(B) Alignment of *let-7* sequences with the 3′ UTRs of the human TGF-βR1.

(C) miRNA expression profiles assessed using quantitative real-time PCR miRNA arrays with cDNA from control or FRS2 knockdown cells.

(D) Quantitative real-time PCR of TGF-βR1 and SM-calponin in HUVECs transduced with Lin28, *let-7* sponge expressing or empty vector. β-actin was used to normalize the variability in template loading.

(E) Immunoblots of TGF-βR1, p-Smad2, Smad2, and FRS2 in control and FRS2 knockdown HUAECs transduced with *let-7* lentiviruses.

(F) Quantitative real-time PCR analysis of TGF-βR1, TGF-β downstream target molecules, smooth muscle marker and mesenchymal marker gene expression in control and FRS2 knockdown HUAECs transduced with *let-7* lentiviruses (*$p < 0.05$; **$p < 0.01$; ***$p < 0.001$ compared to control). β-actin was used to normalize the variability in template loading. Data shown (A and D-F) are representative of three independent experiments.

(G) Mice were injected intravenously with control or cholesterol formulated antagomir-*let-7*b/c (single injection of 2 mg/kg) and the liver endothelial cells were isolated at 6 days. Expression of *let-7* miRNAs were analyzed by quantitative real-time PCR. SNORD66 was used to normalize the variability in template loading (***$p < 0.001$; NS: not significant compared to control).

(H) Gene expression levels of K-ras, N-ras, HMGA2, CDK6, CDC25A, TGF-βR1, and vimentin in liver endothelial cells of mice treated with control or formulated antagomir-*let-7* at 6 days. β-actin was used to normalize the variability in template loading (*$p < 0.05$; ***$p < 0.001$ compared to control).

(I) Immunofluorescence staining of CD31/vimentin (Nuclei were counterstained with DAPI (blue, scale bar: 7 μm.) in liver sections of mice treated with control or formulated antagomir-*let-7* at 6 days.

(J) Quantification of liver ECs expresses vimentin in mice injected with control or formulated antagomir-*let-7* (***$p < 0.001$ compared to control).

See also Figures S3 and S4.

FGF signaling in adult mice can be inhibited by administration of an FGF trap construct (sFGFR1-IIIC) (Murakami et al., 2008). To demonstrate construct effectiveness, exposure of cultured HUVECs to Ad-sFGFR1-IIIc resulted in a distinct morphological change (Figure S4B), suppression of *let-7* expression (Figure S4C), and induction of Endo-MT markers including SM22α,

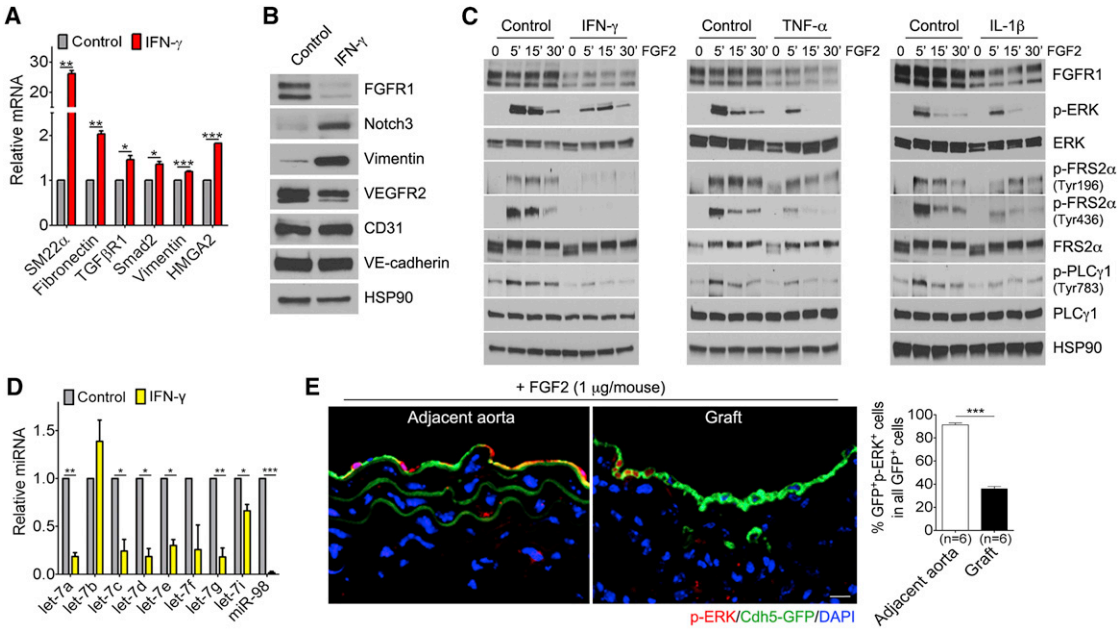

Figure 3. Inflammatory Cytokines (IFN-γ, TNF-α, and IL-1β) Downregulate FGF Receptors, thereby Rendering ECs Less Responsive to FGF In Vitro and In Vivo

(A) Quantitative real-time PCR analysis of smooth muscle and mesenchymal marker gene expression in control and human IFN-γ treated HUVECs (*$p < 0.05$; **$p < 0.01$; ***$p < 0.001$ compared to control). β-actin was used to normalize the variability in template loading.

(B) Immunoblots of smooth muscle and mesenchymal markers in control and human IFN-γ treated HUVECs.

(C) HUVECs were treated with human IFN-γ (10 ng/ml), human TNF-α (10 ng/ml), or human IL-1β (10 ng/ml) in complete growth medium for 6 days followed by incubation in 0.5% FBS starvation medium for 18 hr. Cells were treated with FGF2 (50 ng/ml) for indicated times. Immunoblots of FGF signaling downstream targets.

(D) Quantitative real-time PCR analysis of mature let-7 expression in control and human IFN-γ treated HUVECs. SNORD47 was used to normalize the variability in template loading. Data shown (A–D) are representative of four independent experiments.

(E) Left: Immunofluorescence staining of p-ERK in adjacent aorta and graft sections in Cdh5-CreERT2;mT/mG mice. Scale bar: 10 μm. Right: Quantification of endothelial cell express p-ERK in mice injected with FGF2 (***$p < 0.001$ compared to adjacent aorta).

See also Figures S5 and S6.

SM-calponin, and fibronectin (Figures S4D and S4E). In agreement with these in vitro data, Ad-sFGFR1-IIIc injection into mice led to their detection in the host circulation and a significant reduction in *let-7* miRs expression in primary ECs isolated from hearts and livers of these animals (Figures S4F and S4G).

To determine if reduction in *let-7* expression would have the same effects in vivo as suppression of FGF signaling, we directly targeted *let-7*b and *let-7*c miRNAs in mice using cholesterol formulated antagomirs for improved stability and delivery efficiency (Love et al., 2010). Analysis of *let-7* miRNAs expression 6 days after a single tail vein injection of 2 mg/kg of *let-7*b/c antagomirs in primary liver ECs demonstrated a significant reduction in expression of *let-7*b and *let-7*c miRNA in antagomir-treated compared to control mice while other family members were not affected (Figure 2G). This reduction in *let-7*b/c levels was further confirmed by increased expression of several known *let-7* targets including *K-RAS*, *N-RAS*, *HMGA2*, *CDK6*, and *CDK25A* (Figure 2H). In agreement with the in vitro data, reduction in *let-7*b/c expression led to an increase in TGF-βR1 and vimentin expression (Figure 2H). Finally, immunocytochemical examination of blood vessels in the liver of *let-7* antagomir-treated mice demonstrated increased expression of vimentin in luminal ECs, consistent with Endo-MT (Figures 2I and 2J).

Inflammation-Dependent Suppression of FGF Signaling

The results of the in vitro and in vivo studies presented above demonstrate that decreased FGF signaling leads to reduction in *let-7* expression and initiation of TGF-β-dependent Endo-MT. To demonstrate the relevance of this biology to disease settings, we next examined if Endo-MT occurs in transplant rejection, a process associated with high local interferon-γ (IFN-γ) production that has been reported to suppress FGF signaling (Friesel et al., 1987).

Treatment of HUVECs in culture with IFN-γ led to increased expression of a *let-7*-dependent gene *HMGA2*, an increase in *TGFβR1* and *SMAD2* levels and a large increase in the expression of SMC and other mesenchymal marker expression, including Notch3, SM22α, fibronectin, and vimentin (Figures 3A and 3B). Of note, there was a profound reduction in FGFR1 expression and almost full suppression of FGF signaling (Figure 3C). Treatment of ECs with tumor necrosis factor (TNF)-α and interleukin (IL)-1β led to a similar reduction in FGF signaling (Figure 3C), while other inflammatory cytokines such as IL-6, MCP-1, and VEGF had no such effect (Figures S5A–S5C). In agreement with the observed reduction of FGF signaling, exposure of HUVECs to IFN-γ led to a profound decrease in *let-7* miRs expression (Figure 3D).

We next employed a mouse transplant rejection model characterized by intense local inflammatory responses around the rejecting graft and endothelial fate mapped mice that were generated by crossing *Cdh5-CreER2* and mT/mG ("tomato") mouse lines (both on a C57BL/6 background) followed by activation of the Cre gene by tamoxifen administration from P2 to P20 (Figure S6A). This results in permanent marking of all EC and EC-derived cells with green fluorescent protein (GFP). Analysis of arteries from these mice demonstrated uniform GFP expression in the luminal ECs with a total absence of all SMC (Notch3, αSMA, SM22α) or mesenchymal (vimentin, collagen) markers (Figure S6B).

Engraftment of an aortic segment from BALB/c mice into *Cdh5-CreERT2*-mT/mG (C57BL/6 background) mouse aorta leads to intense graft inflammation and rejection over the next 2–3 weeks. To test the effect of this inflammatory response on endothelial FGF signaling, the mouse hosts of allogeneic artery grafts were intravenously injected with FGF2 at 2 weeks postoperatively and sacrificed 15 min later. Immunocytochemical analysis for FGF signaling demonstrated virtually no p-ERK signal in graft luminal ECs, while luminal ECs from the adjacent normal arterial segment revealed intense p-ERK signal (Figure 3E).

Examination of the graft 2 weeks after transplantation showed that 10.1% of neointimal SMC (defined by expression of either Notch3 or αSMA) expressed GFP, which indicated an endothelial origin (Figures 4A and 4B). Furthermore, a very high proportion of ECs in the neointima (79%) expressed Notch3 and αSMA (Figures 4A and 4C), demonstrating very extensive Endo-MT. To examine the effect of FRS2α expression disruption on this process, we crossed *Frs2*$\alpha^{fl/fl}$ mice onto mT/mG background. FRS2α expression was then inactivated by crossing these mice with Cdh5-CreERT2 driver line (*Cdh5-CreERT2; FRS2*$^{i\Delta EC}$) and then activating Cre expression on postnatal day 5 (P5).

Inhibition of FGF signaling by endothelial-specific *Frs2α* deletion or suppression of *let-7* expression with antagomirs resulted in a further statistically significant ($p < 0.05$) increase in the number of GFP$^+$ SMC (Figures 4A and 4B), while the proportion of neointimal ECs with SMC markers increased to nearly 100% (Figure 4C).

Luminal ECs revealed even more extensive changes: 61% of graft lumen ECs expressed Notch3 and αSMA with the extent of Endo-MT increasing to 80%–90% in *Cdh5-CreERT2; FRS2*$^{i\Delta EC}$ mice or following *let-7* anti-miR administration (Figure 4D). Collagen deposition, another feature of Endo-MT, and neointima thickness of transplanted arteries were significantly increased by both endothelial cell *Frs2α* deletion and *let-7* antagomir treatment (Figures 4E and 4F).

To test the ability of *let-7* miR to rescue this phenotype we used chemically synthesized double stranded *let-7*b miR mimics packaged in liposomal-formulated lipid nanoparticles (LNPs) (Love et al., 2010). The effectiveness of delivery against endothelial targets was assessed by first determining the dose response for inhibition of target gene expression. A single intravenous injection of LNPs carrying from 0.03 to 2.2 mg/kg of *anti-Tie2* siRNA demonstrated 70% inhibition of *Tie2* expression in liver and heart ECs after 72 hr (Figures S7A and S7B) persisting with ~30 day half-life in both organs (Figures S7C and S7D). Similar results were seen with siRNA formulations targeting *Icam2* (Figures S7E and S7F), *Vegfr2* (Figures S7G and S7H), and *Cdh5* (Figures S7I and S7J). In contrast, no detectable reduction of any tested gene was observed with a LNP-formulated luciferase siRNA (LUC) or saline (Figures S7A, S7B, and S7E–S7J), indicating that silencing is specific to the siRNA and is not caused by the liposomal carrier. To demonstrate the physiological significance of this level of inhibition, we carried out an Evans blue assay in mice treated with 0.7 mg/kg of LNP *Cdh5* siRNA. Following knockdown, there was a significant increase in ECs permeability compared to control mice (Figure S7K).

Using the LNP preparation described above, *let-7* mimics (0.5 mg/kg) were injected every other day starting at postoperative day 7 (for a total of four injections) and the grafts were harvested on day 14. Administration of these mimics to grafted mice led to a significant reduction in the number of neointimal SMC of endothelial origin (GFP$^+$/Notch3$^+$ or αSMA$^+$ cells: from 10.1% in the absence of treatment to 3% in mimic-treated mice, $p < 0.05$) (Figures 4A and 4B) as well as in the proportion of neointimal ECs undergoing Endo-MT (from 79% to 20.3%, $p < 0.01$; Figures 4A and 4C). Equally significantly, there was a dramatic decrease in the proportion of luminal ECs undergoing Endo-MT (from 61% to 33.7%, $p < 0.01$; Figures 4A and 4D) and a dramatic reduction in collagen deposition and neointima thickness (Figures 4A, 4E, and 4F).

To determine if a similar phenomenon occurs in human disease, we examined coronary arteries (n = 8) from explanted chronically rejecting hearts. Compared to normal human coronary arteries (Figure 5A), the majority (79.8%) of luminal ECs in arteries procured from patients with chronic cardiac graft rejection expressed the SMC marker, Notch 3 (Figures 5B, 5C, and 5E). Analysis of the neointima showed that similar to the mouse transplant model, Endo-MT was extensive with 76% of neointimal ECs expressing Notch3 (Figures 5D and 5F) and accounted for a significant portion (9.6%) of neointimal SMC (Figure 5G).

Transplantation of a segment of human coronary artery into immunodeficient mouse aorta reconstituted with allogeneic human peripheral blood mononuclear cells (PBMCs) to induce graft rejection (Rao et al., 2008) was then used to verify the occurrence of Endo-MT in human endothelium. Three weeks following PBMC injection, rejecting human arteries demonstrated extensive neointima formation (compare Figure 5H to 5I) and widespread expression of Notch3 in luminal and neointimal ECs (Figures 5J and 5K). Quantitative analysis demonstrated that 84.7% of all luminal and 77% of neointimal ECs expressed Notch3 (Figures 5L and 5M), while 10.4% of neointimal SMC expressed EC markers (Figure 5N).

Finally, to examine the frequency of this phenomenon in other settings, we evaluated two other in vivo models characterized by various extents of neointima formation and vascular inflammation- wire injury and vein-to-artery grafting. Wire injury to the common femoral artery in *Cdh5-CreERT2;mT/mG* mice resulted in neointima development with 5.2% of neointimal cells demonstrating GFP expression (Figure 6A). Grafting mouse vena cava into the aorta of syngeneic *Cdh5-CreERT2;mT/mG* mice was also associated with evidence of Endo-MT in the neointima 3% at 2 weeks and 6.7% at 4 weeks. Luminal ECs of the vein graft also displayed extensive Endo-MT with 31% expressing

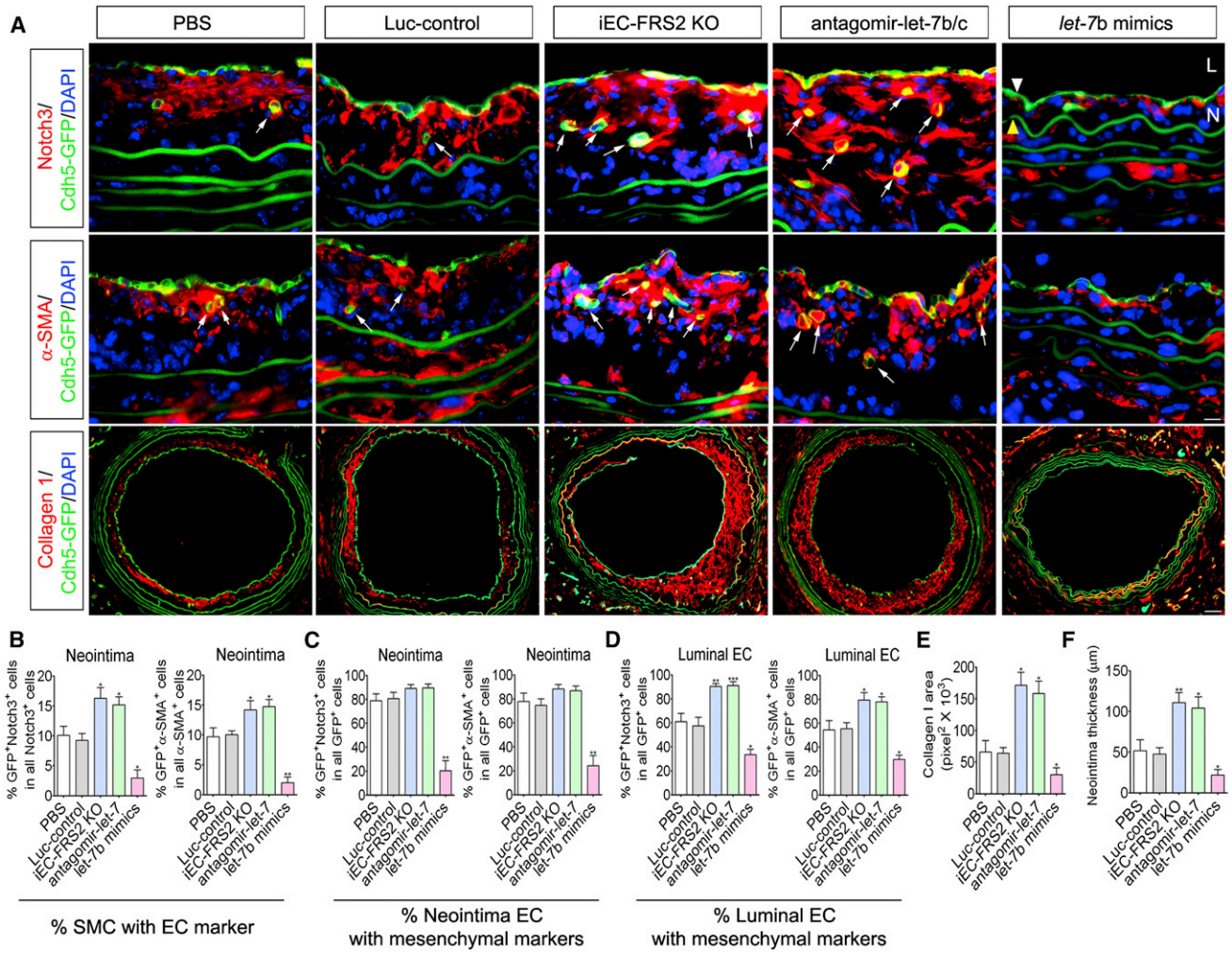

Figure 4. Endo-MT Participates in Mouse Arteriosclerosis

(A) Histological analysis of artery grafts by immunostaining with anti-Notch3, anti-αSMA, and anticollagen 1. Cdh5-GFP$^+$/Notch3$^+$ (red) and Cdh5-GFP$^+$/αSMA$^+$ (red) colocalization indicates Endo-MT and appears yellow. Nuclei were counterstained with DAPI (blue). Scale bar: 10 μm for Notch3 and αSMA and 63 μm for collagen 1. L, lumen; N, neointima; white triangle indicates endothelial cells; yellow triangle indicates IEL (internal elastic lamina); arrows indicate endothelial cells express SMC markers.

(B) Percentage of Notch3$^+$ (left) or αSMA$^+$ (right) cells that were Cdh5-GFP$^+$ in neointima (*$p < 0.05$; **$p < 0.01$ compared to control).

(C) Percentage of Cdh5-GFP$^+$ cells that were Notch3$^+$ (left) or αSMA$^+$ (right) in neointima (**$p < 0.01$ compared to control).

(D) Percentage of Cdh5-GFP$^+$ cells that were Notch3$^+$ (left) or αSMA$^+$ (right) in lumen (*$p < 0.05$; **$p < 0.01$; ***$p < 0.001$ compared to control).

(E and F) Morphometric assessment of collagen 1 area and artery graft neointima thickness was performed by computer-assisted microscopy (*$p < 0.05$; **$p < 0.01$ compared to control). PBS (n = 7 mice/group), Luc-control (n = 6 mice/group), *Cdh5-CreERT2; Frs2*$^{i\Delta EC}$ (n = 4 mice/group), antagomir-*let-7* (n = 9 mice/group), and *let-7*b mimics (n = 6 mice/group).

See also Figure S7.

mesenchymal markers 2 weeks after grafting and 45.6% after 4 weeks (Figure 6B).

DISCUSSION

The data in the present study indicate that basal FGF signaling in ECs is required to maintain *let-7* miRNA expression. High *let-7* levels, in turn, are required for suppression of TGF-β signaling and inhibition of Endo-MT. Finally, Endo-MT itself is an important contributor to the development of neointima in a number of disease states characterized by FGF signaling resistance. Thus, FGF control of *let-7* expression directly regulates TGF-β signaling, links these two critical growth factor signaling pathways, and maintains the normal state of the vasculature (Figure 7).

FGFs exert a plethora of effects on a large number of cell types (Eswarakumar et al., 2005). In the vascular system, FGF signaling plays a protective role with ongoing FGF stimulation required for the maintenance of vascular system integrity (Hatanaka et al., 2011; Murakami et al., 2008) and VEGFR2 expression (Murakami

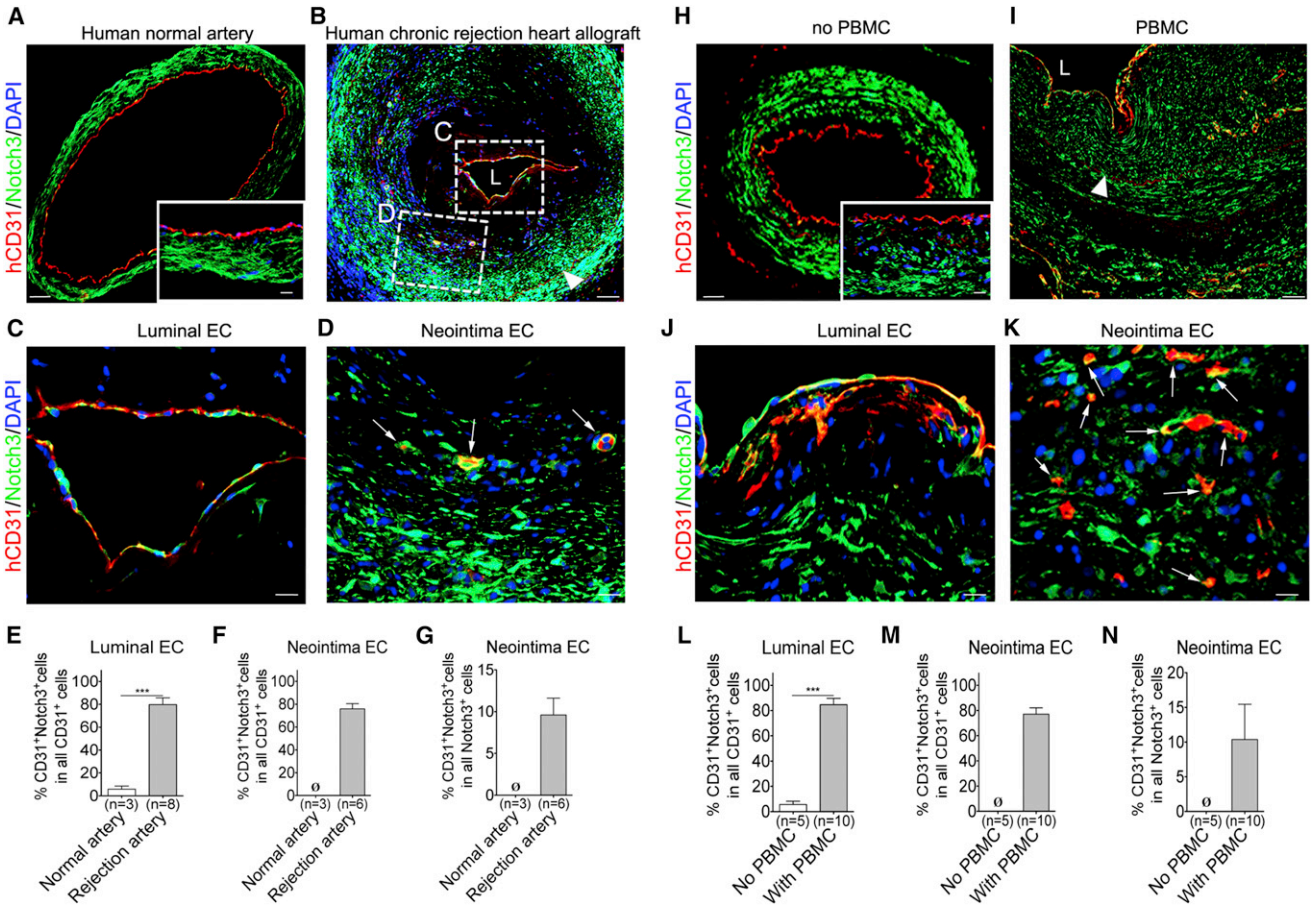

Figure 5. Endo-MT Participates in Human Graft Arteriosclerosis

(A and B) Representative images of human CD31 and Notch3 immunofluorescent staining of human normal and chronically rejecting human coronary arteries. Scale bar: 62 μm. L indicates lumen; white triangle indicates IEL (internal elastic lamina).

(C and D) High-power images of human chronic rejection coronary artery lumen and neointima ECs colocalized with Notch3 staining. Scale bar, 16 μm. Arrows indicate endothelial cells express SMC markers.

(E) Percentage of $CD31^+$ cells that were $Notch3^+$ in lumen (***$p < 0.001$ compared to normal artery).

(F) Percentage of $CD31^+$ cells that were $Notch3^+$ in neointima (Ø, not detected).

(G) Percentage of $Notch3^+$ cells that were $CD31^+$ in neointima (Ø, not detected).

(H and I) Representative images of human CD31 and Notch3 immunofluorescent staining of human coronary artery transplants in SCID/beige mice reconstituted with or without human PBMCs. Scale bar: 62 μm. L indicates lumen; white triangle indicates IEL (internal elastic lamina).

(J and K) High-power images of artery graft treated with human PBMC lumen and neointima ECs colocalized with Notch3 staining. Scale bar: 16 μm. Arrows indicate endothelial cells express SMC markers.

(L) Percentage of $CD31^+$ cells that were $Notch3^+$ in lumen (***$p < 0.001$ compared to no PBMC).

(M) Percentage of $CD31^+$ cells that were $Notch3^+$ in neointima (Ø, not detected).

(N) Percentage of $Notch3^+$ cells that were $CD31^+$ in neointima (Ø, not detected).

et al., 2011). The current study expands this FGF function by demonstrating the role of ongoing FGF signaling in prevention of Endo-MT and implicates *let-7* miRNA as the key player in this process.

let-7 miRNA family was originally identified in *Caenorhabditis elegans* as a regulator of developmental timing and cell proliferation (Reinhart et al., 2000). The family is highly conserved across the entire phylogenetic tree and in mice and humans it consists of 11 very closely related genes encoded on three different chromosomes (Roush and Slack, 2008). To date, *let-7* miRs have been implicated in the control of numerous events during embryogenesis including nervous system and liver development (Maller Schulman et al., 2008), tumor suppression (Zhang et al., 2007), and inhibition of cell proliferation (Johnson et al., 2007), while recent studies have indicated their involvement in EMT in tumors including a suggestion that an increase in *let-7*b levels reverses this process (Li et al., 2009). *let-7* miRNAs are also highly expressed in ECs and are considered proangiogenic (Urbich et al., 2008).

Despite these important biological roles, little is known about the regulation of *let-7* biogenesis. During embryonic development, RNA binding proteins LIN28a/b selectively block its

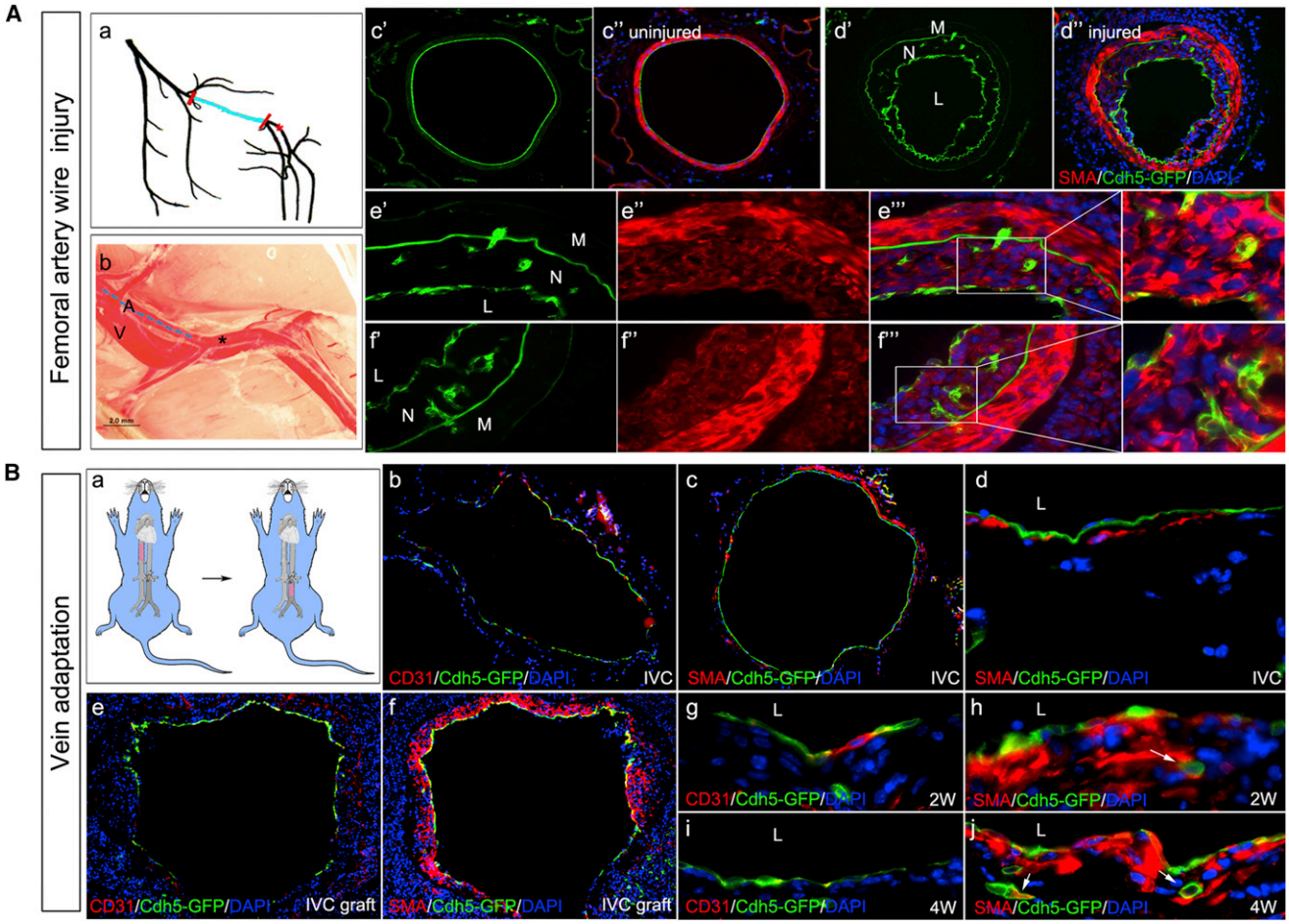

Figure 6. Endo-MT in Femoral Artery Wire Injury and Vein Adaptation Models

(A) (a and b) Anatomy of the hindlimb vasculature. Blue lines indicate denuded endothelium layer. A, artery; V, vein; asterisks indicate wire inserted site. (c and d) Representative images of cross sections of the uninjured (left) and injured (right) femoral arteries. (e and f) Immunofluorescence staining of αSMA (red) in injured femoral artery sections 3 weeks after injury. L, lumen; N, neointima; M, media.

(B) (a) Schematic of vein to artery grafting. (b and c) Immunofluorescence staining of CD31 (red) and αSMA (red) in low power magnification of inferior vena cava (IVC). (d) Immunofluorescence staining of αSMA (red) in high power magnification of IVC. (e and f) Immunofluorescence staining of CD31 (red) and αSMA (red) in low power magnification of vein grafts. (g–i) Immunofluorescence staining of CD31 (red) in high power magnification of vein grafts 2 and 4 weeks after transplantation. (h and j) Immunofluorescence staining of αSMA (red) in high-power magnification of vein grafts 2 or 4 weeks after transplantation.

maturation (Hagan et al., 2009; Lehrbach et al., 2009), while a heteronuclear ribonucleoprotein A1 (hnRNPA1) inhibits its processing by DROSHA (Michlewski and Cáceres, 2010). LIN28 is not expressed in the adult endothelium and we observed no increase in hnRNPA1 expression after FGF blockade (data not shown). Our data suggest that homeostatic FGF stimulation is essential for continued *let-7* expression but the mechanism of this effect is uncertain. *let-7* family, in turn, has been indirectly linked to the regulation of several TGF-β family members including TGF-βR1 (Tzur et al., 2009).

Our study provides strong evidence supporting the link between FGF signaling, *let-7* expression, and TGF-β. In cell culture studies, suppression of FGF signaling using several different approaches uniformly resulted in a marked (up to 120-fold) decrease in *let-7* expression. In vivo, *let-7* levels were dramatically decreased in embryos with reduced FGF signaling (*Frs2α-2F* mutants), while systemic administration of a pan-FGF trap, sFGFR1-IIIc, reduced *let-7* levels in endothelial cells from different organs. In each case, loss of FGF signaling-dependent *let-7* expression was associated with increased TGF-β family member expression, activation of TGF-β signaling and the appearance of Endo-MT markers.

The fact that the change in *let-7* levels itself and not some other effect of blocking FGF signaling is responsible for the up-regulation of TGF-β signaling and Endo-MT is supported by a number of observations. In vitro studies show that reduction in *let-7* expression in ECs induced by antagomirs, a pan-*let-7* sponge or expression of the *let-7* suppressor LIN28A leads to increased expression of TGF-β, TGF-βR1, and classic TGF target genes such as collagen or vimentin. Furthermore, ECs demonstrated a dramatic morphological change consistent with Endo-MT and expression of a number of smooth muscle

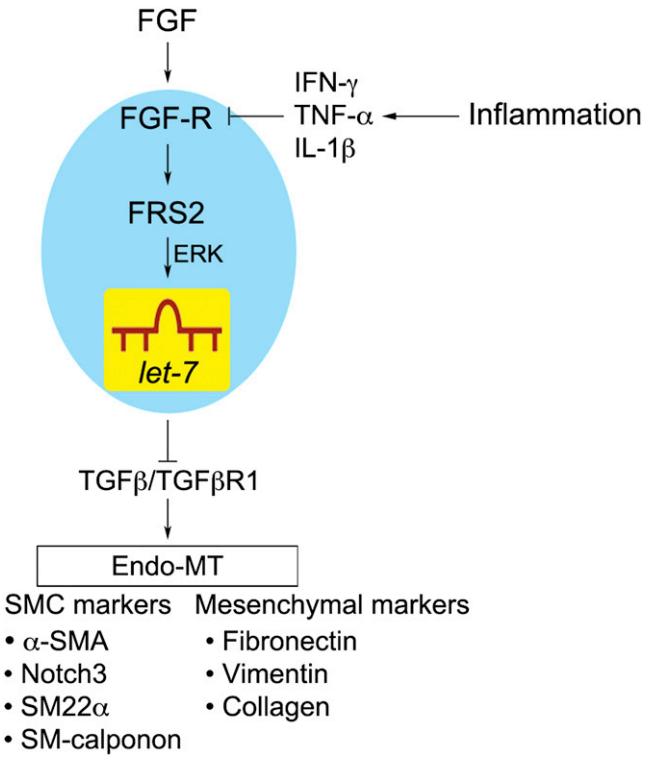

Figure 7. Schema of FGF-Dependent Regulation of TGF-β Signaling and Endo-MT

and other mesenchymal markers. Similarly, in vivo antagomir suppression of *let-7*b/c expression also led to increased TGF-βR1 expression and appearance of Endo-MT markers. Most importantly, restoration of *let-7*b levels in the endothelium using modified *let-7*b mimics and a delivery system designed to facilitate miRNA delivery to the endothelium, reversed the effect of FGF blockade or *let-7* antagomir treatment on expression of Endo-MT markers and its functional consequences. While all *let-7* family members are expressed in ECs, we chose *let-7*b because it demonstrates, along with *let-7*c, the most dramatic reduction in expression upon FGF signaling withdrawal and because of all *let-7* *let-7*b has the best complementarity with *TGFβR1* (Tzur et al., 2009).

The existence of an Endo-MT phenomenon still remains a matter of intense debate as are its contributions to human pathology. In addition to TGF-β, two other signaling pathway, Notch (Chang et al., 2011) and Tie-1 (Garcia et al., 2012), have also been reported to induce it. The molecular details, however, remain sparse. While there is a significant body of evidence linking TGF-β signaling to EMT, its role in Endo-MT is much less established. Several studies have reported that a prolonged stimulation of ECs in vitro with TGF-β can induce Endo-MT (Zeisberg et al., 2007a) but there are no studies demonstrating the ability of TGF-β to induce Endo-MT in vivo. TGF-β is thought to induce Endo-MT via SMAD-dependent activation of SNAIL (Kitao et al., 2009). Endo-MT has been reported to occur in the setting of cardiac, renal, pulmonary, cancer and age-related fibrosis (Ghosh et al., 2010; Zeisberg et al., 2007a, 2007b). The current study strongly supports the reality of an Endo-MT phenomenon and expands its biological role.

In particular, we have demonstrated that Endo-MT plays an important role in neointima formation, a process underlying a number of important cardiovascular disease states. In the transplant model, Endo-MT accounted for ~10% of SMC in the neointima, while ~80% of luminal ECs demonstrated mesenchymal transition. This is highly significant as, so transformed, these cells can be expected to secrete large amounts of collagen and other ECM proteins thus contributing to vessel fibrosis. Indeed, extensive fibrosis was evident in endothelial-specific *Frs2α* deletion or *let-7* antagomir administration. Furthermore, the acquisition of a mesenchymal phenotype by luminal ECs is likely to lead to endothelial dysfunction, such as an increase vascular permeability or potentiate leukocyte transmigration (Murakami et al., 2008).

The trigger for the occurrence of Endo-MT is the loss of FGF signaling. While many factors can and do affect this process, the occurrence of FGF resistance is clearly associated with inflammation. We traced this link to the ability of key inflammatory mediators, including IFN-γ and TNF-α, to reduce FGFR1 expression and markedly decrease FGF-dependent ERK activation. Thus, conditions associated with intense vascular inflammation such as allogeneic artery transplantation, induce an extensive Endo-MT response. In other models of vascular injury where the loss of FGF signaling is less profound, such as wire artery injury or vein-to-artery grafting, Endo-MT still occurs but to a more limited extent. Beyond vascular injury, Endo-MT has been reported in a number of pathological settings including acute myocardial infarctions (Zeisberg et al., 2007b) and acute kidney injury (Basile et al., 2011) that are also characterized by an intense inflammatory component.

Most importantly, Endo-MT clearly occurs in human disease. Indeed, eight out of eight human arteries from chronically rejecting cardiac allografts demonstrated clear evidence of Endo-MT and human arteries transplanted into immunodeficient mice reconstituted with allogeneic human PBMC underwent Endo-MT with the same frequency as allogeneic mouse artery grafts.

In summary, FGF regulates endothelial TGF-β signaling by controlling TGF-β, TGF-βR1, and SMAD2 expression via control of *let-7* levels. The emergence of an FGF resistance state and a reduction in FGF signaling input leads to a profound decrease in *let-7* levels and increased TGF-β signaling culminating in Endo-MT that, in turn, leads to neointima formation and fibrosis.

EXPERIMENTAL PROCEDURES

Primary Mouse Endothelial Cell Isolation and Culture

Primary mouse endothelial cells were isolated from the heart and liver as described (Murakami et al., 2011).

let-7 Family Microsponge Construction

A *let-7* microsponge of 273 nt was constructed containing nine bulged binding sites (one for each of the *let-7* family members: *let-7a*, *let-7b*, *let-7c*, *let-7d*, *let-7e*, *let-7f*, *let-7g*, *let-7i*, and mir-98). The *let-7* family microsponge was synthesized by the annealing and ligation of six single-strand chemically synthesized DNA fragments. The bulged binding sites were designed using the canonic rules for microRNA binding sites (Filipowicz et al., 2008). The 273 nt *let-7* family microsponge was subcloned in tandem to multiply the binding sites.

Western Blot Analysis

Cells were lysed with T-PER (Thermo Scientific) containing complete mini protease inhibitors (Roche) and phosphatase inhibitors (Roche). Total protein (20 μg) from each sample was resolved on a 4%–12% Bis-Tris Gel (Bio-Rad) with MOPs Running Buffer (Bio-Rad), transferred to nitrocellulose membranes (Bio-Rad) and probed with antibodies. Chemiluminescence measurements were performed using SuperSignal West Femto Maximum Sensitivity Substrate (Thermo Fisher Scientific).

RNA Isolation, Quantitative Real-Time PCR, and Gene Expression Profiling

RNA was isolated using RNeasy plus Mini Kit (QIAGEN) and converted to cDNA using iScript cDNA synthesis kit (Bio-Rad). Quantitative real-time PCR was performed using Bio-Rad CFX94 (Bio-Rad) by mixing equal amount of cDNAs, iQ SYBR Green Supermix (Bio-Rad), and gene-specific primers. All reactions were done in a 25 μl reaction volume in duplicate. Data were normalized to endogenous β-actin. Primers are listed in Table S1. Quantitative real-time PCR analysis of 84 TGF-β-related and EMT-related genes was performed using Human TGF-β BMP signaling pathway (PAHS-035D, QIAGEN) RT^2 Profiler PCR Arrays and run on a Bio-Rad CFX96 machine (Bio-Rad). Data analysis was done using manufacturer's integrated web-based software package with cycle threshold (Ct)-based fold-change calculations.

MicroRNA Target Prediction

To identify potential miRNA binding sites within the 3′UTR of *TGFβR1*, the following bioinformatic databases were used: TargetScan (http://www.targetscan.org), PitTar (http://pictar.mdc-berlin.de), and DIANA-microT v3.0 (http://diana.cslab.ece.ntua.gr/).

microRNA Real-Time PCR Analysis

Quantitative real-time PCR analysis of 88 miRNA was performed using Human Cell Differentiation & Development RT^2 Profiler PCR Arrays (MAH-103A, QIAGEN). Validation of microRNA array data was performed with the RT^2 miRNA qPCR Assays and RT-PCR Primer Sets (QIAGEN). Individual miRNA expression was normalized in relation to expression of small nuclear *SNORD47* (for human) or *Snord66* (for mouse). PCR amplification consisted of 10 min of an initial denaturation step at 95°C, followed by 45 cycles of PCR at 95°C for 30 s, 60°C for 30 s.

Generation of Mice and Embryos

$Frs2^{flox/flox}$ (Lin et al., 2007) and *Frs2α-2F* (Gotoh et al., 2004) mice were previously described. *Cdh5-CreERT2* (gift from R.H. Adams, Max Planck Institute, Munster) transgenic mice were crossed with mT/mG [B6,129(Cg)-Gt(ROSA)$26Sor^{tm4(ACTB-tdTomato,-EGFP)Luo}$/J] (JAX SN:007676) mice to generate EC-specific reporter mice. For fate mapping of Cdh5-GFP expressing cells, *Cdh5CreERT2;mT/mG* pups were pipette-fed with 0.05 mg/g tamoxifen solution (20 mg/ml stock solution in corn oil) every other day ten times.

let-7 miRNA Lipid Formulation

Synthesis of let-7b Antagomirs

Antagomirs to *let-7*b and *let-7*c were synthesized as described (Krützfeldt et al., 2005): anti-*let-7*b, 5′- $a_s a_s$ccacacaaccuacuacc$_s u_s c_s a_s$-Chol-3′; and anti-*let-7*c, 5′ $a_s a_s$ccauacaaccuacuacc$_s u_s c_s g_s$-Chol-3′. The lowercase letters represent 2′-*O*Me-modified nucleotides; subscript "s" represents a phosphorothioate linkage; and "Chol" represents cholesterol linked through a hydroxyprolinol linkage. Anti-*let-7*b and anti-*let-7*c were encapsulated in LNPs using the same method and composition as previously described for C12-200-siRNA formulations (Love et al., 2010). Particle size was determined by dynamic light scattering (Zetasizer Nano ZS; Malvern, UK). The mean diameter for anti-*let7*b-LNP was 145 nm and for anti-*let7*c-LNP was 160 nm.

Synthesis of let-7b Mimics

Chemically modified miRNA mimics were synthesized at Alnylam Pharmaceuticals (Cambridge, MA). The sequences for the mature strands of *let-7*b after processing by DICER, mmu-*let-7*b-5p (mmu-*let-7*b, MIMAT0000522), and mmu-*let-7*b-3p (mmus-*let-7*b*, MIMAT0004621), were obtained from the miRbase (http://www.miRbase.org). 2-*O*-methyl-nucleotide modifications (indicated in lowercase) were introduced to both strands to decrease the likelihood of triggering an innate immune response. Double-stranded miRNA mimics were obtained after annealing equimolar amounts of the chemically modified 5p and 3p strands: mi-*let-7*b_L, for lightly modified (5p 5′-UGAGGuAGuAG GUUGUGUGGUU-3′, 3p 5′-CuAuAcAACCuACUGCCUUCCC-3′); and mi-*let-7*b_H, for heavily modified, (5p 5′-UGAGGuAGuAGGUUGUGUGGUU-3′, 3p 5′-cuAuAcAAccuAcuGccuuccc-3′). LNPs formulated with siRNA targeting luciferase, siLuc, were used as control.

miRNA Formulation in Lipid Nanoparticles

microRNA mimics and siLuc were encapsulated in LNPs formulated with the lipid C12-200, using the same protocol and composition as previously described. The mean diameter range for all LNPs was 54–59 nm.

In Vivo sFGFR1-IIIc Adenovirus Administration and let-7 Antagomir Delivery

sFGFR1-IIIc adenovirus (Murakami et al., 2008) was administered at a dose of 5×10^{10} viral particles per mouse via lateral tail vein injection. Control mice were given equivalent volumes of sterile PBS. Serum level of sFGFR1-IIIc was measured by a Human IgG Subclass Profile kit (Invitrogen). For *let-7* antagomir delivery, mice were administered with either 1:1 mixture of anti-*let7*b-LNP and anti-*let7*c-LNP or PBS at 2 mg/kg body weight in 0.1 ml per injection via lateral tail vein. Measurements of miRNA or mRNA levels in ECs were performed 6 days after the injection.

In Vivo let-7 Antagomir and let-7 Mimics Delivery in Mouse Arterial Transplant Model

For *let-7* experiment, 7 days after arterial transplant, mice were injected with four doses of *let-7* antagomir (2 mg/kg), luciferase-control (0.5 mg/kg), and *let-7*b mimics (0.5 mg/kg) in 0.1 ml per injection via jugular vein every other day.

Human Tissue

Deidentified human coronary arteries were obtained from organ donors with normal cardiac function, from end-stage cardiomyopathy patients undergoing heart transplantation, or from cardiac allograft recipients with chronic rejection at autopsy or undergoing retransplantation. Tissue collection and analysis was approved by the review boards of Yale University School of Medicine, the New England Organ Bank, and the University of British Columbia.

Endo-MT Animal Models

All experiments were performed under protocols approved by Yale University Institutional Animal Care and Use and Human Investigation Committees.

Arterial Transplant Models

For mouse to mouse major mismatch arterial transplant model, segments of thoracic aorta from male, 4- to 5-week-old BALBc/J mice were interposed into the infrarenal aortae of male recipient, 10- to 12-week-old *Cdh5CreERT2;mT/mG* mice using an end-to-end microsurgical anastomotic technique.

For human to mouse arterial transplant model, adjacent segments of human coronary artery from surgical specimens or cadaveric organ donors were implanted into the infrarenal aortae of 8- to 12-week-old CB.17 severe combined immunodeficient (SCID)/beige mice. The animals received 1×10^8 human allogeneic (to the artery) PBMCs per mouse, injected intraperitoneally 1 week after transplantation. Animals were euthanized 4 weeks after coronary artery transplantation and transplanted arteries were removed and frozen in optimal cutting temperature (OCT) compound (Tissue-Tek) for further analysis.

Femoral Artery Injury Model

This was done as described previously (Acevedo et al., 2004).

Vein Graft Model

For mouse vein to artery grafting model, segments of intrathoracic inferior vena cava from male, 4- to 5-week-old C57BL/6 mice were interposed into the infrarenal aortae of male recipient, 10- to 12-week-old *Cdh5CreERT2;mT/mG* mice using an end-to-end microsurgical anastomotic technique.

Morphometric Analysis

To harvest transplanted grafts, artery, or liver, animals were anesthetized and tissues were perfused with normal saline and 4% paraformaldehyde (PFA). For cryosection preparation, grafts were isolated from anesthetized mice, fixed in 4% PFA overnight at 4°C, cryoprotected 6 hr in 15% sucrose at 4°C, and embedded in OCT (Tissue-Tek).

Immunofluorescence Staining

Frozen blocks were sectioned at 6 μm intervals. For frozen tissue sections, slides were fixed in acetone for 10 min at −20°C. For paraffin sections, slides were dewaxed in xylene, and antigen retrieval was performed by boiling for 20 min in citrate buffer (10 mM [pH 6.0]) and rehydrated. After washing three times with PBS, tissue sections were incubated with the following primary antibodies diluted in blocking solution (10% BSA and horse serum in PBS) overnight at 4°C in a humidified chamber: anti-human SM α-actin-APC (1:10); rabbit anti-Notch3 (1:100); rabbit anti-collagen 1 (1:100); rabbit anti-SM22α (1:100). Sections were washed three times with TBS, incubated with appropriate Alexa Fluor 488, 594, or 633 conjugated secondary antibodies diluted 1:1,000 in blocking solution for 2 hr at room temperature, washed again three times, and mounted on slides with Prolong Gold mounting reagent with DAPI (Invitrogen). Images were captured using Velocity software and quantifications performed using ImageJ (NIH).

Computer Assisted Image Analysis (Quantitative IF)

Procollagen and collagen positive area were measured using NIH Image 1.60. Neointima thickness was measured from 4 regions of a section along a cross, calculated the average from 5 serial cross-sections, 150 μm apart for each graft, using computer-assisted image analysis and NIH Image 1.60. For evaluation of $\alpha SMA^+/Cdh5\text{-}GFP^+$ or $Notch3^+/Cdh5\text{-}GFP^+$ cells, at least ten sections 150 μm apart per graft were analyzed for colocation of endothelial and smooth muscle markers using immunofluorescent staining imaged under 10× magnification.

Statistical Analysis

Analysis was performed using GraphPad Prism software v.5. All data are presented as mean ± SD, and two group comparisons were done with a two-tailed Student's t test. A value of $p < 0.05$ was taken as statistically significant.

SUPPLEMENTAL INFORMATION

Supplemental Information includes Extended Experimental Procedures, seven figures, and one table and can be found with this article online at http://dx.doi.org/10.1016/j.celrep.2012.10.021.

LICENSING INFORMATION

ACKNOWLEDGMENTS

We thank R. Friesel (Maine Medical Center Research Institute) for providing FGFR1 constructs and FGFR1 antibody, R. Adams (Max Planck Institute, Munster) for Cdh5-CreERT2 mouse, V. Eswarakumar (Yale University) for the gift of *Frs2α*-2F mice, N. Kirkiles-Smith (Yale University) for technical assistance with i.v. injections, B. McManus (University of British Columbia) for human coronary artery specimens, and S. Kuchimanchi (Alnylam) for miR mimics synthesis. This work was supported by National Institutes of Health Grants R01-HL 053793 (to M.S.) and R01-CA 131301 (to F.J.S.). P.-Y.C., L.Q., G.T., and M.S. conceived and designed the experiments and discussed the results. P.-Y.C., L.Q., T.Y., X.Z., R.A., and J.Y. performed experiments. P.P.M. and F.J.S. generated and provided *let-7* sponge construct, F.W. generated *Frs2* knockin mouse, and C.B., K.C., D.G.A., and V.K. developed in vivo delivery system and generated and provided *let-7* anti-miRs for in vivo studies. P.-Y.C., G.T., and M.S. wrote the manuscript. C.B., K.C., and V.K. were employees of Alnylam, Inc. when this work was performed.

Received: May 22, 2012
Revised: October 6, 2012
Accepted: October 26, 2012
Published: November 29, 2012

REFERENCES

Acevedo, L., Yu, J., Erdjument-Bromage, H., Miao, R.Q., Kim, J.E., Fulton, D., Tempst, P., Strittmatter, S.M., and Sessa, W.C. (2004). A new role for Nogo as a regulator of vascular remodeling. Nat. Med. *10*, 382–388.

Basile, D.P., Friedrich, J.L., Spahic, J., Knipe, N., Mang, H., Leonard, E.C., Changizi-Ashtiyani, S., Bacallao, R.L., Molitoris, B.A., and Sutton, T.A. (2011). Impaired endothelial proliferation and mesenchymal transition contribute to vascular rarefaction following acute kidney injury. Am. J. Physiol. Renal Physiol. *300*, F721–F733.

Chang, A.C., Fu, Y., Garside, V.C., Niessen, K., Chang, L., Fuller, M., Setiadi, A., Smrz, J., Kyle, A., Minchinton, A., et al. (2011). Notch initiates the endothelial-to-mesenchymal transition in the atrioventricular canal through autocrine activation of soluble guanylyl cyclase. Dev. Cell *21*, 288–300.

Chen, P.Y., Simons, M., and Friesel, R. (2009). FRS2 via fibroblast growth factor receptor 1 is required for platelet-derived growth factor receptor beta-mediated regulation of vascular smooth muscle marker gene expression. J. Biol. Chem. *284*, 15980–15992.

Costa, M.A., and Simon, D.I. (2005). Molecular basis of restenosis and drug-eluting stents. Circulation *111*, 2257–2273.

Eswarakumar, V.P., Lax, I., and Schlessinger, J. (2005). Cellular signaling by fibroblast growth factor receptors. Cytokine Growth Factor Rev. *16*, 139–149.

Fafeur, V., Terman, B.I., Blum, J., and Böhlen, P. (1990). Basic FGF treatment of endothelial cells down-regulates the 85-KDa TGF beta receptor subtype and decreases the growth inhibitory response to TGF-beta 1. Growth Factors *3*, 237–245.

Filipowicz, W., Bhattacharyya, S.N., and Sonenberg, N. (2008). Mechanisms of post-transcriptional regulation by microRNAs: are the answers in sight? Nat. Rev. Genet. *9*, 102–114.

Friesel, R., Komoriya, A., and Maciag, T. (1987). Inhibition of endothelial cell proliferation by gamma-interferon. J. Cell Biol. *104*, 689–696.

Garcia, J., Sandi, M.J., Cordelier, P., Binétruy, B., Pouysségur, J., Iovanna, J.L., and Tournaire, R. (2012). Tie1 deficiency induces endothelial-mesenchymal transition. EMBO Rep. *13*, 431–439.

Ghosh, A.K., Bradham, W.S., Gleaves, L.A., De Taeye, B., Murphy, S.B., Covington, J.W., and Vaughan, D.E. (2010). Genetic deficiency of plasminogen activator inhibitor-1 promotes cardiac fibrosis in aged mice: involvement of constitutive transforming growth factor-beta signaling and endothelial-to-mesenchymal transition. Circulation *122*, 1200–1209.

Gotoh, N., Ito, M., Yamamoto, S., Yoshino, I., Song, N., Wang, Y., Lax, I., Schlessinger, J., Shibuya, M., and Lang, R.A. (2004). Tyrosine phosphorylation sites on FRS2alpha responsible for Shp2 recruitment are critical for induction of lens and retina. Proc. Natl. Acad. Sci. USA *101*, 17144–17149.

Hagan, J.P., Piskounova, E., and Gregory, R.I. (2009). Lin28 recruits the TUTase Zcchc11 to inhibit let-7 maturation in mouse embryonic stem cells. Nat. Struct. Mol. Biol. *16*, 1021–1025.

Hatanaka, K., Simons, M., and Murakami, M. (2011). Phosphorylation of VE-cadherin controls endothelial phenotypes via p120-catenin coupling and Rac1 activation. Am. J. Physiol. Heart Circ. Physiol. *300*, H162–H172.

Johnson, C.D., Esquela-Kerscher, A., Stefani, G., Byrom, M., Kelnar, K., Ovcharenko, D., Wilson, M., Wang, X., Shelton, J., Shingara, J., et al. (2007). The let-7 microRNA represses cell proliferation pathways in human cells. Cancer Res. *67*, 7713–7722.

Khurana, R., Zhuang, Z., Bhardwaj, S., Murakami, M., De Muinck, E., Yla-Herttuala, S., Ferrara, N., Martin, J.F., Zachary, I., and Simons, M. (2004).

Angiogenesis-dependent and independent phases of intimal hyperplasia. Circulation *110*, 2436–2443.

Kitao, A., Sato, Y., Sawada-Kitamura, S., Harada, K., Sasaki, M., Morikawa, H., Shiomi, S., Honda, M., Matsui, O., and Nakanuma, Y. (2009). Endothelial to mesenchymal transition via transforming growth factor-beta1/Smad activation is associated with portal venous stenosis in idiopathic portal hypertension. Am. J. Pathol. *175*, 616–626.

Krützfeldt, J., Rajewsky, N., Braich, R., Rajeev, K.G., Tuschl, T., Manoharan, M., and Stoffel, M. (2005). Silencing of microRNAs in vivo with 'antagomirs'. Nature *438*, 685–689.

Lehrbach, N.J., Armisen, J., Lightfoot, H.L., Murfitt, K.J., Bugaut, A., Balasubramanian, S., and Miska, E.A. (2009). LIN-28 and the poly(U) polymerase PUP-2 regulate let-7 microRNA processing in Caenorhabditis elegans. Nat. Struct. Mol. Biol. *16*, 1016–1020.

Li, Y., VandenBoom, T.G., 2nd, Kong, D., Wang, Z., Ali, S., Philip, P.A., and Sarkar, F.H. (2009). Up-regulation of miR-200 and let-7 by natural agents leads to the reversal of epithelial-to-mesenchymal transition in gemcitabine-resistant pancreatic cancer cells. Cancer Res. *69*, 6704–6712.

Lin, Y., Zhang, J., Zhang, Y., and Wang, F. (2007). Generation of an Frs2alpha conditional null allele. Genesis *45*, 554–559.

Love, K.T., Mahon, K.P., Levins, C.G., Whitehead, K.A., Querbes, W., Dorkin, J.R., Qin, J., Cantley, W., Qin, L.L., Racie, T., et al. (2010). Lipid-like materials for low-dose, in vivo gene silencing. Proc. Natl. Acad. Sci. USA *107*, 1864–1869.

Maller Schulman, B.R., Liang, X., Stahlhut, C., DelConte, C., Stefani, G., and Slack, F.J. (2008). The let-7 microRNA target gene, Mlin41/Trim71 is required for mouse embryonic survival and neural tube closure. Cell Cycle *7*, 3935–3942.

Medici, D., Potenta, S., and Kalluri, R. (2011). Transforming growth factor-β2 promotes Snail-mediated endothelial-mesenchymal transition through convergence of Smad-dependent and Smad-independent signalling. Biochem. J. *437*, 515–520.

Michlewski, G., and Cáceres, J.F. (2010). Antagonistic role of hnRNP A1 and KSRP in the regulation of let-7a biogenesis. Nat. Struct. Mol. Biol. *17*, 1011–1018.

Murakami, M., Nguyen, L.T., Zhuang, Z.W., Moodie, K.L., Carmeliet, P., Stan, R.V., and Simons, M. (2008). The FGF system has a key role in regulating vascular integrity. J. Clin. Invest. *118*, 3355–3366.

Murakami, M., Nguyen, L.T., Hatanaka, K., Schachterle, W., Chen, P.Y., Zhuang, Z.W., Black, B.L., and Simons, M. (2011). FGF-dependent regulation of VEGF receptor 2 expression in mice. J. Clin. Invest. *121*, 2668–2678.

Ohtani, K., Egashira, K., Hiasa, K., Zhao, Q., Kitamoto, S., Ishibashi, M., Usui, M., Inoue, S., Yonemitsu, Y., Sueishi, K., et al. (2004). Blockade of vascular endothelial growth factor suppresses experimental restenosis after intraluminal injury by inhibiting recruitment of monocyte lineage cells. Circulation *110*, 2444–2452.

Papetti, M., Shujath, J., Riley, K.N., and Herman, I.M. (2003). FGF-2 antagonizes the TGF-beta1-mediated induction of pericyte alpha-smooth muscle actin expression: a role for myf-5 and Smad-mediated signaling pathways. Invest. Ophthalmol. Vis. Sci. *44*, 4994–5005.

Ramos, C., Becerril, C., Montaño, M., García-De-Alba, C., Ramírez, R., Checa, M., Pardo, A., and Selman, M. (2010). FGF-1 reverts epithelial-mesenchymal transition induced by TGF-beta1 through MAPK/ERK kinase pathway. Am. J. Physiol. Lung Cell. Mol. Physiol. *299*, L222–L231.

Rao, D.A., Eid, R.E., Qin, L., Yi, T., Kirkiles-Smith, N.C., Tellides, G., and Pober, J.S. (2008). Interleukin (IL)-1 promotes allogeneic T cell intimal infiltration and IL-17 production in a model of human artery rejection. J. Exp. Med. *205*, 3145–3158.

Reinhart, B.J., Slack, F.J., Basson, M., Pasquinelli, A.E., Bettinger, J.C., Rougvie, A.E., Horvitz, H.R., and Ruvkun, G. (2000). The 21-nucleotide let-7 RNA regulates developmental timing in Caenorhabditis elegans. Nature *403*, 901–906.

Roush, S., and Slack, F.J. (2008). The let-7 family of microRNAs. Trends Cell Biol. *18*, 505–516.

Tzur, G., Israel, A., Levy, A., Benjamin, H., Meiri, E., Shufaro, Y., Meir, K., Khvalevsky, E., Spector, Y., Rojansky, N., et al. (2009). Comprehensive gene and microRNA expression profiling reveals a role for microRNAs in human liver development. PLoS ONE *4*, e7511.

Urbich, C., Kuehbacher, A., and Dimmeler, S. (2008). Role of microRNAs in vascular diseases, inflammation, and angiogenesis. Cardiovasc. Res. *79*, 581–588.

Viswanathan, S.R., and Daley, G.Q. (2010). Lin28: A microRNA regulator with a macro role. Cell *140*, 445–449.

Zeisberg, E.M., Potenta, S., Xie, L., Zeisberg, M., and Kalluri, R. (2007a). Discovery of endothelial to mesenchymal transition as a source for carcinoma-associated fibroblasts. Cancer Res. *67*, 10123–10128.

Zeisberg, E.M., Tarnavski, O., Zeisberg, M., Dorfman, A.L., McMullen, J.R., Gustafsson, E., Chandraker, A., Yuan, X., Pu, W.T., Roberts, A.B., et al. (2007b). Endothelial-to-mesenchymal transition contributes to cardiac fibrosis. Nat. Med. *13*, 952–961.

Zhang, B., Pan, X., Cobb, G.P., and Anderson, T.A. (2007). microRNAs as oncogenes and tumor suppressors. Dev. Biol. *302*, 1–12.